CrossMark

RESEARCH PAPER

Comparison of the characteristics of rock salt exposed to loading and unloading of confining pressures

Jie Chen · Deyi Jiang · Song Ren · Chunhe Yang

Abstract Rock mechanical behaviors and deformation characteristics are associated with stress history and loading path. Unloading conditions occur during the formation of a salt cavity as a result of washing techniques. Such conditions require an improved understanding of the mechanical and deformation behaviors of rock salt. In our study, rock salt dilatancy behaviors under triaxial unloading confining pressure tests were analyzed and compared with those from conventional uniaxial and triaxial compression tests. The volume deformation of rock salt under unloading was more than under triaxial loading, but less than under uniaxial loading (with the same deviatoric stress). Generally, under the same axial compression, the corresponding dilatancy rate decreased as the confining compression increased, and under the same confining compression, the corresponding dilatancy rate increased as the axial compression increased. The dilatancy boundary of the unloading confining pressure test began with unloading. This is different from the dilatancy of the uniaxial and triaxial compression tests. The accelerated dilatancy point boundary stress value was affected by confining and axial compressions. The specimens entered into a creep state after unloading. The associated creep rate depends on the deviatoric stress and confining compression values at the end of the unloading process. Based on unloading theory and the experimental data, we propose a constitutive model of rock salt damage.

Our model reflects the dilatancy progression at constant axial stress and reduced lateral confinement.

Keywords Dilatancy · Loading path · Rock salt · Triaxial · Uniaxial · Unloading

1 Introduction

Subterranean energy storage is an effective approach for solving the seasonal variation of energy consumption. Rock salt, which has very low permeability and porosity, good creep behavior, and forms under natural hydrogeological conditions, is a suitable medium for the storage of gas, crude oil and radioactive waste. Underground cavities leached in salt domes and salt beds have been used extensively for storing hydrocarbons in North America, Europe, and Asia [10, 18, 22]. The mechanical behavior of natural rock salt has been investigated experimentally [1, 3, 4, 9, 12, 20, 24]. These works focused on the mechanical properties of uniaxial and triaxial compression and creep, but little attention has been paid to the unloading process.

Stress redistribution induced by underground excavation results in unloading zones in the surrounding rock [6, 15]. The mechanical behavior of rock under unloading is different from those under loading [5, 17, 21, 23]. Therefore, it is essential to investigate the mechanical behaviors of rock salt to ensure cavity stability. Unloading failure was first reported by Poncelet [2] who investigated the failure process in glass specimens subjected to uniaxial compression. In specimens that were not loaded to catastrophic failure, as the load was removed, many small cracks formed at the interface between the loading platen and the glass specimen. While characterizing single crystal quartz under uniaxial compression, Kimberley et al. [11] observed

J. Chen (✉) · D. Jiang · S. Ren · C. Yang
State Key Laboratory for Coal Mine Disaster Dynamics and Controls, Chongqing University, Chongqing 400030, People's Republic of China
e-mail: chenjie_cqu@163.com

J. Chen · C. Yang
Institute of Rock and Soil Mechanics, Chinese Academy of Science, Wuhan, Hubei 430071, People's Republic of China

the initiation and growth of cracks during the removal of the applied loads from specimens. They inferred that residual stresses from inelastic strains accumulate during loading. These residual stresses are relieved through creep if the load is removed slowly, but if the load is removed quickly, then the stresses are released through crack initiation and growth. Under the same initial stress conditions, the change in magnitude of stress required for rock failure is less than that of the triaxial compressive process [7, 8]. The plastic deformation of salt rock is different from the brittle failure of hard rock under the unloading of confining pressure.

To investigate the mechanical behaviors of rock salt under unloading conditions, uniaxial and triaxial compression tests and triaxial unloading tests were carried out on standard rock salt test specimens from Pakistan. Rock salt dilatancy behavior in the triaxial unloading of confining pressure test was compared with that from conventional uniaxial and triaxial compression tests. Based on unloading theory, a constitutive model of rock salt damage was obtained.

2 Experimental method

2.1 Specimens

Typically, rock salt forms colorless or white isometric crystals; however, they might also be light blue, dark blue, purple, pink, red, orange, yellow, or gray, depending on the amount and type of impurities. In many cases, evaporation of rock salt occurs due to evaporated deposit minerals, such as sulfates, halides, and borates. To minimize the effects of impurities on our results, high purity salt from the Khewra salt mine in Pakistan was used in this study. Khewra salt mine is located in Khewra, north of Pind Dadan Khan, Pakistan, which is approximately 288 m above sea level and 730 m into the mountain. The test specimens were pink, transparent, and compact. The soluble content ranged from 96.3 to 99.8 % (soluble substances mainly NaCl, Na_2SO_4), and the insoluble compositions were mainly argillic minerals. The specimens used in the tests were cylindrical with a diameter of 50 mm and length up to 100 mm, and the samples were cut and processed in strict accordance with rock mechanic test standards (Fig. 1).

2.2 Procedures

With the progressive excavation in a salt cavern, the horizontal stress around the excavation boundary releases, breaking original in situ stress balance and resulting in the redistribution of vertical stress. We therefore, initially applied triaxial loading. Then, once the surrounding

Fig. 1 Manufactured salt sample and installation method

pressure approached a given three-dimensional stress state, the axial load was held constant and the surrounding stress reduced slowly. This simulates the state of decreasing surrounding pressure and increasing deviatoric stress in the surrounding rock during excavation.

The following tests were carried out:

1. Conventional uniaxial and triaxial compression tests and triaxial unloading confining pressure tests. The rock salt deformation and failure behavior during the unloading of confining pressure was determined.
2. The analysis of rock salt dilatancy characteristics under unloading confining pressure (initial axial compression of 25 MPa). Three different initial surrounding pressures were selected: 10, 15, and 20 MPa. At an initial confining pressure of 25 MPa, four different initial axial compressions were selected: 20, 25, 30, and 35 MPa, which required the same unloading rates and test steps.
3. To analyze the mechanical deformation behavior of rock salt after unloading, the axial compression was maintained at 30 MPa. After the surrounding pressure approached 0 MPa from 15 or 5 MPa, rock salt creep characteristics were observed.

The loading and unloading steps in the triaxial unloading compression tests were as follows.

1. Loading section: The surrounding pressure was increased (at a rate of 0.02 MPa/s) to maxima of 15, 20, or 25 MPa. Then, the axial load was increased (at a rate of 0.02 MPa/s) until 20, 25, 30, or 35 MPa was attained. The axial and confining pressures were then kept constant for 1 min prior to unloading.
2. Unloading section: This simulates the evolution of stresses during unloading, while the axial pressure remained unchanged and the surrounding pressure was reduced. The axial load was held constant at 25 MPa, and the surrounding pressure was reduced gradually to

0 MPa (at a rate of 0.005 MPa/s). (N.B. the unloading rate is relatively small during a long period of excavation.)

3 Results and discussion

3.1 Dilatancy characteristics of rock salt

Three groups of rock salt specimens were selected for tests conducted at room temperature, and the results are shown in Figs. 2, 3 and 4. The progression of volumetric strain can be divided into three stages: a volume compression stage, a steady-state dilatancy stage, and an accelerated dilatancy stage. The common characteristics of rock salt
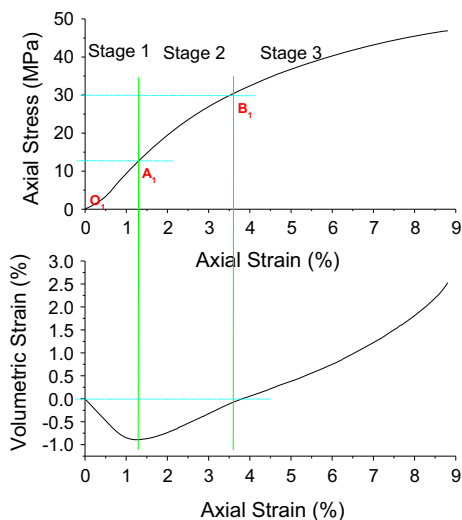
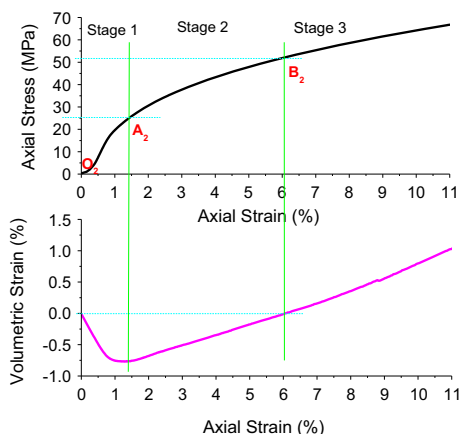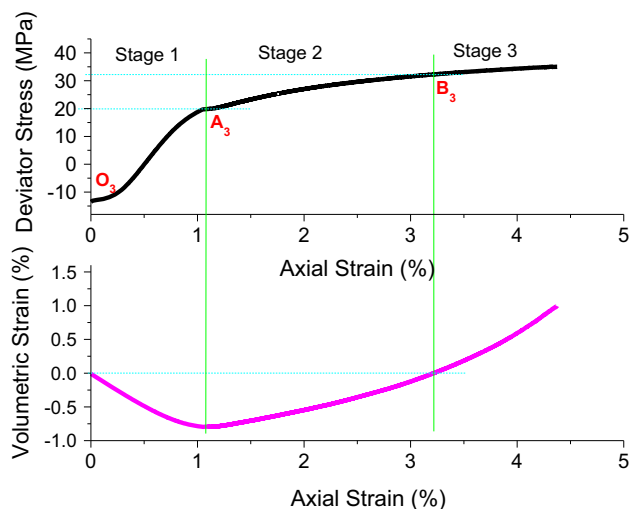**Fig. 4** General stress–strain relationship of the unloading confining pressure test

dilatancy under three kinds of load paths can be described as follows.

Stage 1 (O_iA_i, $i = 1$, 2 and 3. Volume compression stage): The rock salt specimen is compressed and its volume reduced as the deviatoric stress increases. During this stage, pores and fractures are abundant in the rock specimens. During early loading, volume compression always results in the closure of fractures. Following deformation, the cracks open and grow, and this is characterized by the departure of the strain curves from linearly elastic behavior. The rate of increase is higher for axial strain, which indicates that the volume change from crack opening is predominantly in the direction of the shear stress. Although this stage is referred to as the stable crack growth region because of controlled crack development, the volumetric strain decreases.

Stage 2 (A_iB_i, $i = 1$, 2 and 3. Steady-state dilatancy stage): The specimen volume expands from its primary compression when the deviatoric stress approaches point A. Point A is the onset of dilatancy or the compression–dilatancy (C/D) boundary. The stable crack growth process and the final elastic deformation overlap at the dilatancy boundary. At this point of maximum compression, the gradient of the volumetric strain curve is reversed. The magnitude of the dilatancy boundary depends on the minimal stress component. The volume of the specimen increases gradually, and the rock salt behavior changes from elastic to plastic, indicating that the primary closed fractures reopen. As the deviatoric stress increases, the crystal particles interact, and the spaces between the crystal particles expand, prompting the formation and development of new fractures. At this

Fig. 2 General stress–strain relationship of the uniaxial compression test

Fig. 3 General stress–strain relationship of the triaxial compression test

point, the permeability of the rock salt does not increase and a cluster network of cracks develops. For this reason, the dilatancy at point B is called the "percolation dilatancy" [19].

Stage 3 (B$_{i-}$, $i = 1$, 2 and 3. Accelerated dilatancy stage): The growth of the cracks continues, and the sample volume expands to its original value at point B. The volumetric strain increases. The rock salt exhibits viscoplastic deformation, and this affects its permeation characteristics. The deviatoric stress increases sufficiently to break the bonds within the crystal particles; thus, regular sliding is more chaotic (diastrophism), and the new fractures and microcracks combine to create bigger fractures. The crack growth process is irreversible and unstable, representing the short-term plastic behavior of rock salt under a deviatoric stress regime.

3.1.1 Volume compression behavior in the three loading paths

The compression stage (OA) in Figs. 2, 3, 4 and 5 shows different characteristics in the volume deformation curves and stress–strain curves of the three loading paths.

In the uniaxial and triaxial compression test, the curve of the compression stage is downwardly concave as a result of the initial closure of inner fractures and elastic deformation. In the triaxial unloading confining pressure test, the volumetric strain curve is approximately flat in the loading period. Before the axial load is applied, the consolidation stage ends; thus, the rock salt is subjected to elastic compression. As the tests focus on the unloading stage, the rate of loading to attain the initial three-dimensional stress state is fast. The lower compression limits of the specimens
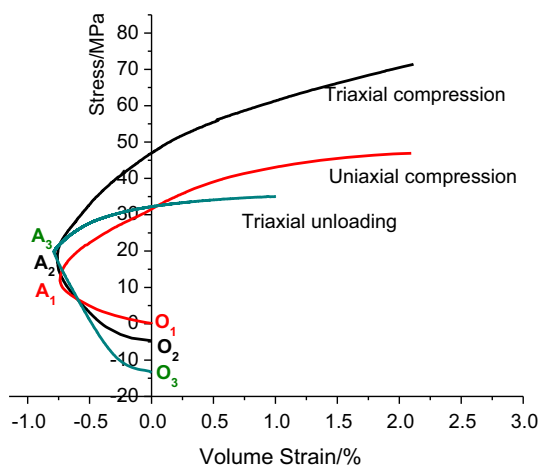

Fig. 5 Stress–volumetric strain *curves* of specimens. *Point* O$_3$ denotes the volume compression induced by the confining pressure of 15 MPa; loading in the vertical direction is zero

(points A$_1$, A$_2$, and A$_3$) in the three-dimensional stress state are approximately the same (volumetric strain is 0.78 %). The compressed volume of the specimens is mainly the interspace volume. If rocks have similar lithologies and inner fractures, then the compression volume ratio is almost the same after the fractures are completely closed.

3.1.2 Dilatancy boundary points in the three loading paths

Figures 2, 3, 4 and 5 show that the dilatancy boundary points of the three loading modes are different.

1. In the uniaxial compression test, as the stress reaches the ultimate elastic strength of the specimen, the specimen volume expands and plastic deformation occurs, inducing new fractures and expanding inner pores. The dilatancy points are associated with the specimen's elastic limit. The uniaxial dilatancy boundary point is determined from the point of the ultimate elastic strength on stress–strain curves.

2. In the triaxial compression test, plastic deformation occurs before the dilatancy boundary point. Full compression of the pore volume occurs before dilatancy. The dilatancy boundary stress decreases with increasing loading rate and increasing pore pressure, which accelerates the expansion of the rock mass. Alkana et al. [19] found that rock salt triaxial dilatancy boundary values are related to octahedral shear stress as follows:

$$\tau = \tau_{max}\left(\frac{b\sigma}{1 + b\sigma}\right) \tag{1}$$

where σ is average stress, τ is the octahedral shear stress, τ_{max} is the peak shear stress, and b is a constant.

3. In the triaxial unloading test, it is easy to determine the dilatancy boundary value. Inner pores are consolidated under early loading confining pressure and axial load. When the loading is stopped, if the stress state is kept constant, then the inner pore volume remains unchanged. However, once unloading commences and the applied confining pressure is reduced, dilatancy occurs. In the triaxial compression tests, it was difficult to attain full compression of the pore volume, as the dilatancy boundary point occurs just as the unloading process starts. During the excavation of salt caverns, water-leaching technology is applied. This leads to a redistribution of the cavity confining pressure, which is similar to unloading. The surrounding rock of the cavity expands in volume. As we have shown in Fig. 5, specimen failure occurs more rapidly in triaxial unloading tests than in triaxial compression tests; therefore, we should pay more attention to the potential for disasters caused by unloading in salt cavern projects.

3.1.3 Dilatancy processes in the three loading paths

The volume dilatancy stage AB shows various characteristics for the different loading paths. After dilatancy occurs, the volumetric strain exhibits a linear trend against axial strain. Axial strain ranged from 1.23 to 3.59 %, from 1.17 to 3.28 %, and from 1.43 to 6.12 % in the uniaxial tests, unloading tests, and triaxial tests, respectively.

The dilatancy extent from points A to B is different under the same deviatoric stress. The rate of damage evolution and dilatancy extent is large under the uniaxial compression test. The proportion of AB dilatancy in the entire dilatancy process in the uniaxial test is large compared with the unloading test. Steady-state dilatancy in the uniaxial compression test was caused by pores expanding, and accelerated dilatancy opens old cracks and generates new cracks. This process is based upon non-conservative deformation during loading, which might lead to local tensile stresses during unloading [19]. However, it also involves a time-dependent mechanism (creep), which results in the rate dependence of the unloading failure.

The dilatancy extent of the triaxial compression test was larger than that of both the unloading and uniaxial tests. Microstructural observations confirmed that deformation occurred by dislocation glide, with grain boundary microcracking in the dilatant field. Although many grains experience dislocation glide during triaxial compression, the constant confining pressure could reduce lateral deformation. Dilatancy also depends on stress loading rate, time, and temperature.

A critical factor in the unloading test was the varying confining pressure. The mode of regulating the unloading stress easily leads to dilatancy. Dilatancy is related to deviatoric stress, but is more closely related to confining pressure. Under the same deviatoric stress, dilatancy is confined at some levels by the confining pressure.

3.1.4 Damage behavior in the three loading paths

In the uniaxial tests, the tiny microcracks (Fig. 6a) resulting from tensile and shear failure connect with each other to form fractures. In the triaxial compression tests, the compressive volumetric deformation under confining compression is relatively large, and bulging occurs, accompanied by many tiny cracks (Fig. 6b). However, despite such large volumetric deformation, the rock salt still maintains its rheological behavior. At low confining pressures, creep-type pressure shear failure occurs in the triaxial compression tests, and at high confining pressures, bulging fractures occur. For the triaxial unloading tests, throughout the entire unloading process, the axial compression is held constant with decreasing confining pressure (Fig. 6c). This is a "transitional" stress state, between the uniaxial compressive failure

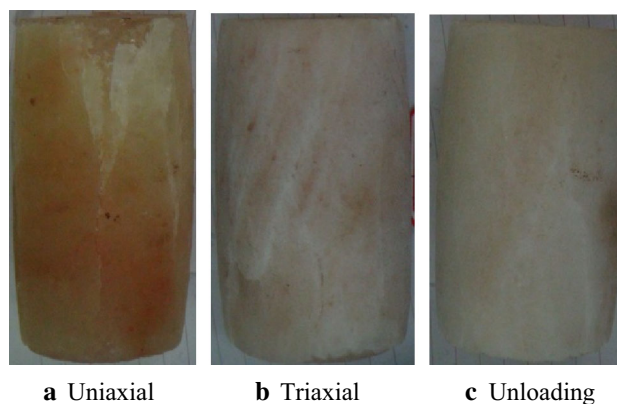
a Uniaxial **b** Triaxial **c** Unloading

Fig. 6 Failure characteristics of rock salt specimens in the three loading paths

mode and the triaxial compressive failure mode; shear failure with tension cracks occur. Note that the failure modes in the three loading paths depend on the experimental set-up conditions. Further, the loading rate and rock environment affect the failure mode of rock salt. Therefore, our conclusions focus on the stress states.

3.2 Dilatancy rate characteristics of rock salt in unloading tests

In the triaxial unloading tests, as the confining pressure decreases, the corresponding deviatoric stress increases at a constant rate. In the early stage of unloading, the deviatoric stress is relatively small, because the initial confining pressure is large, and therefore, volumetric strain slowly changes. The rate of increase in volumetric strain follows a linear trend. As the unloading process continues, the confining pressure is reduced and the deviatoric stress increases along with the rock salt volumetric strain. In Figs. 7, 8, 9, and 10, the volumetric strain rate, which is
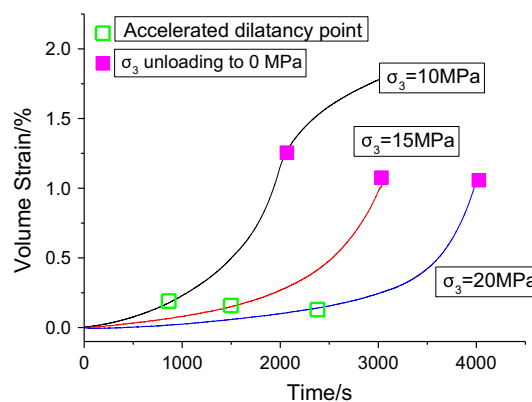

Fig. 7 Time–volumetric strain relationship with constant σ_1 and variable σ_3. In this figure, the initial volumetric strain is zero; i.e., the volumetric strain is zero at the unloading initiation point (cf. *point* A in Fig. 5)
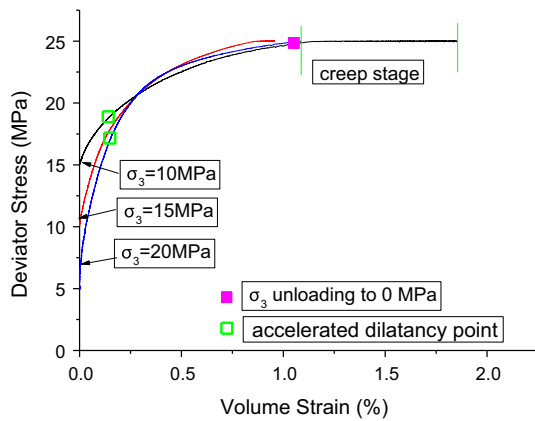
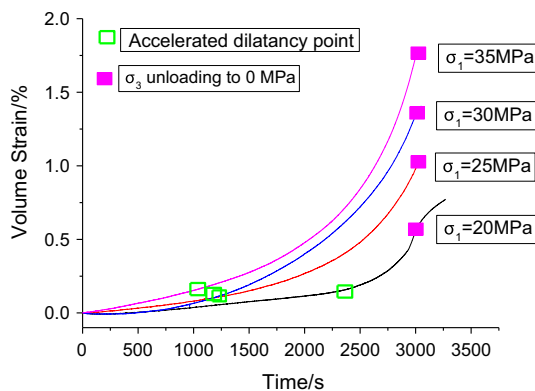**Fig. 8** Deviatoric stress–volumetric strain relationship with constant σ_1 and variable σ_3

Fig. 9 Time–volumetric strain relationship with constant σ_3 and different σ_1
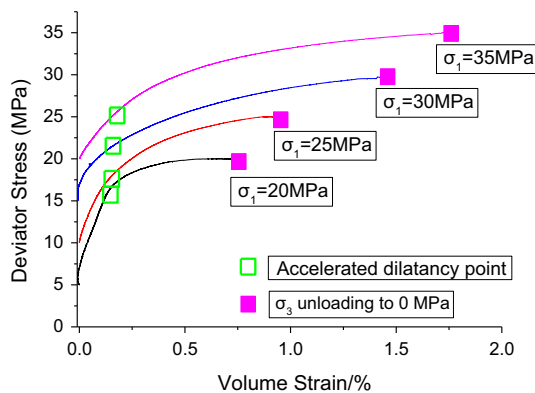

Fig. 10 Deviatoric stress–volumetric strain relationship with constant σ_3 and variable σ_1

approximately linear during the early stages, appears to accelerate in the later stages, as defined at accelerated dilatancy points. The corresponding deviatoric stress is referred to as accelerated dilatancy critical stress. When the confining pressure is reduced to zero, and the test continues, then creep deformation occurs (cf. the 10 MPa curve

in Fig. 7). The stress, volumetric strain, and volumetric strain rates of the unloading tests for different initial confining pressures and different initial axial compressions are listed in Table 1.

3.2.1 Influence of initial confining pressure on dilatancy rate

Figure 7 shows the strain–time curves for different initial confining pressures with the same initial axial compression. The deviatoric stress with time (and also deviatoric stress with volumetric strain) is linear at constant unloading rates. For lower initial confining pressures and fast dilatancy rates, the corresponding dilatancy rates of the accelerated dilatancy point decreases as the confining pressure increases (cf. Table 1; Figs. 7, 8). Under the same initial axial compression, when accelerated dilatancy occurs, the critical deviatoric stress and critical confining pressure are approximately the same, and the corresponding volumetric strains are similar. When the volumetric strain approaches 0.24 % and the critical confining pressure is 4.88 MPa, the deviatoric stress and volumetric strain curves for the three deviatoric stress conditions are similar, and the three different initial stress states become the same. At later stages, the volumetric strain rate also shows the same trend after the confining pressure is reduced to zero. Under the same initial axial compression, as the different initial confining compressions decrease to a certain value, the confining pressure and axial compression states are the same. Additionally, the unloading rates are the same and thus similar stress–strain behaviors are observed.

3.2.2 Effects of initial axial compression on dilatancy rates

Under the same initial confining compressions and different initial axial compressions, the same stress unloading rates are applied, and the rock salt volumetric strain rate increases with initial axial compression (cf. Table 1; Figs. 8, 9). The dilatancy rate increases with the initial axial compression. Because different initial axial compressions occur under the same initial confining compression conditions, when the confining compression is zero, the final deviatoric stress is directly related to axial compression. With a larger initial axial compression and larger deviatoric stress, the corresponding volumetric strain rate is large at zero confining compression.

3.2.3 Discussion of the dilatancy rate of rock salt in a triaxial unloading test

The rate of volumetric strain change against time in the triaxial unloading test was determined from the creep tests

Table 1 Unloading test data for different initial axial pressures and initial confining pressures

Serial number	Initial axial pressure (MPa)	Initial confining pressure (MPa)	Coordinates of accelerated dilatancy point		Volumetric strain (%)	Dilatancy rate of accelerated dilatancy point (ε_v s^{-1})
			Critical deviatoric stress (MPa)	Critical confining pressure (MPa)		
XW-1	25	10	18.87	6.13	0.15	1.57×10^{-4}
XW-2	25	15	17.47	7.53	0.145	1.13×10^{-4}
XW-3	25	20	16.82	8.18	0.135	5.35×10^{-5}
XZ-1	20	15	15.82	4.18	0.133	5.66×10^{-5}
XZ-2	25	15	17.47	7.53	0.142	7.87×10^{-5}
XZ-3	30	15	23.54	6.46	0.134	8.48×10^{-5}
XZ-4	35	15	25.31	9.69	0.16	1.13×10^{-4}

conducted after the unloading process was complete. In Fig. 11, the volumetric strain is observed to increase linearly before the accelerated dilatancy point, and nonlinearly after this point. Additionally, the unloading stage is much shorter than the creep stage. For large initial deviatoric stresses, the rock salt dilatancy rate under the unloading test occurs in two stages: the unloading stage and the creep stage. After the unloading process, the specimen starts to creep. The creep process in the triaxial compression test comprises an initial creep stage and a steady-state creep stage. The relationship between rock salt volumetric strain and time is divided into three stages:

$$\varepsilon_I = d_1 e^{d_2 t} \quad \text{unloading stage AC}$$
$$\varepsilon_{II} = \varepsilon_c - \alpha(1 - e^{d_3 t}) \quad \text{initial creep stage CD} \quad (2)$$
$$\varepsilon_{III} = \varepsilon_D + \beta t \quad \text{steady-state creep stage D}$$

where ε_I is the strain of stage AC (the unloading stage); ε_{II} is the strain of stage CD (the initial creep stage); ε_{III} is the strain after point D (the steady-state creep stage); ε_c is the

strain at point C; ε_D is the strain at point D; t is time; d_1, d_2 and d_3 are constants; the coefficients α and β related to the deviatoric stress. Taking the derivative of Eq. (2) with respect to time, the rock salt dilatancy rate under the unloading process is:

$$\dot{\varepsilon}_I = d_1 d_2 e^{d_2 t} \quad \text{unloading stage AC}$$
$$\dot{\varepsilon}_{II} = -\alpha d_3 e^{d_3 t} \quad \text{initial creep stage CD} \quad (3)$$
$$\dot{\varepsilon}_{III} = \beta \quad \text{steady-state creep stage}$$

The volumetric strain change rate under initial confining and axial compression has the following features. (1) Under the same initial axial compression, the volumetric strains caused by different confining compressions are approximately the same. Only the volumetric strain rate at the early unloading stage is reduced slightly as the initial confining compression is increased. (2) While the initial confining compression is constant, the corresponding volumetric strain rate increases with growing initial axial compression, and at the same time, the corresponding dilatancy volume increases. (3) Under a given stress state, if the confining pressure in the final stage of unloading is not less than the critical deviatoric stress, then the specimen dilatancy rate will depend on the initial deviatoric stress dilatancy rate. (4) Under a given stress state, while the confining compression is reduced to a critical value, accelerated dilatancy occurs, and when it is reduced to zero, the specimen shows uniaxial mode creep. If the confining pressure is unloaded to a certain value and then kept constant, the resulting creep deformation will be similar to that which occurs in the triaxial compression state. This process is similar to the unloading process of salt cavity construction using water-leaching techniques. With continuous water leaching, the confining compression gradually reduces and the surrounding rock volume expands. The brine pressure exhibits a certain protective effect, which means that the rock salt is always under the triaxial unloading process and that the rate of dilatancy is low. (5) When the unloading process is completed, the
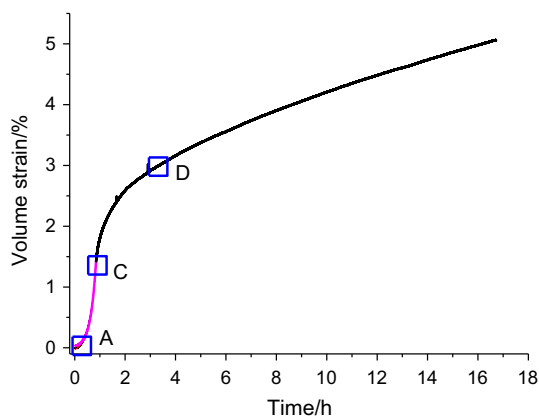

Fig. 11 Time–volumetric strain *curves* for rock salt from unloading to creep. It shows the test *curve* of the unloading and creep processes. *Point* A indicates the start of unloading, *point* C is where unloading is complete, and *point* D is the transition from initial creep to steady-state creep

creep stage occurs, with the creep deformation rate related to the deviatoric stress.

3.3 Boundary conditions of an accelerated dilatancy point under unloading conditions

Rock salt has an accelerated dilatancy point under unloading conditions (Table 1). The accelerated dilatancy point boundary under triaxial unloading and the dilatancy boundary in the triaxial compression test can be defined in similar ways. First, the mean stress and the octahedral shear stress are determined (Alkana et al. [19]):

$$\sigma_m = \frac{1}{3}(\sigma_1 + 2\sigma_2) \tag{4}$$

$$\bar{\sigma} = |\sigma_1 - \sigma_2| = \frac{3}{\sqrt{2}}\tau \tag{5}$$

where σ_m (both here and in the following formulas) is the mean stress, σ_1 is the maximum principal stress, σ_2 is the minimum principal stress, $\bar{\sigma}$ is the absolute deviatoric stress, and $\sigma_2 = \sigma_3$ for a cylindrical specimen, τ (again both here and in the following formulas) is the octahedral shear stress. If $\sigma_1 > \sigma_2$, then Eq. (4) can be rewritten as:

$$\sigma_1 = \sigma_m + \frac{2}{3}\bar{\sigma} = \sigma_m + \sqrt{2}\tau \tag{6}$$

or

$$\sigma_2 = \sigma_m - \frac{\bar{\sigma}}{3} = \sigma_m - \frac{\sqrt{2}}{2}\tau \tag{7}$$

Figure 12 shows that under constant axial compression and reduced confining compression, the corresponding accelerated point boundary is related to the initial stress state. We also surmise that the geological environment of rock salt (i.e., temperature, moisture content, pore water pressure) and its structure affect accelerated point boundary values. The dilatancy boundary relationship under unloading conditions is

$$\tau = k_1\sigma_m \tag{8}$$

where k_1 is a constant.

Equation (8) has the same form as the triaxial dilatancy formula, proposed by Spiers and Carter [16]. They proved that the accelerated dilatancy point boundary in the unloading process had a similar dilatancy mechanism to the dilatancy boundary in general triaxial compression tests.

3.4 A rock salt constitutive model based on unloading theory

Figure 13 shows a typical deviatoric stress–strain curve in an unloading test. Segment AC is the unloading dilatancy stage, at point C, unloading is completed (confining
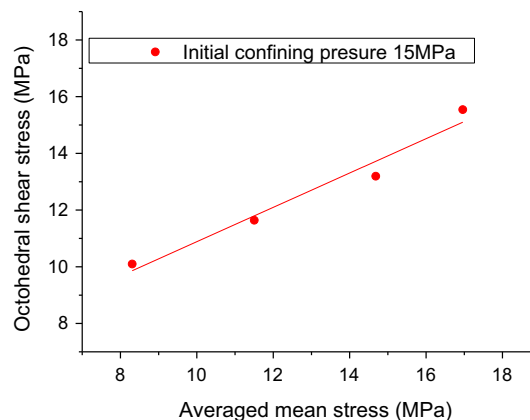
Fig. 12 Accelerated dilatancy *curves* for rock salt determined from unloading test data

compression is zero and axial loading is unchanged), segment CD is the initial creep stage, and a steady-state creep stage occurs after point D.

The constitutive models of specimens at different stages of the unloading test were analyzed.

3.4.1 Unloading dilatancy stage

The AC stage curve in Fig. 13 was fitted to the constitutive equation (Eq. 9) of rock salt under the triaxial unloading stage:

$$\sigma = \sigma_1 - \sigma_3 = \sigma_A + \frac{\eta\varepsilon}{k_2 + \varepsilon} \tag{9}$$

where σ is the deviatoric stress (with the same meaning in the following formulas), σ_1 is axial stress, σ_3 is confining pressure, ε is axial strain, σ_A is the initial deviatoric stress when the unloading process began and η and k_2 are constants.
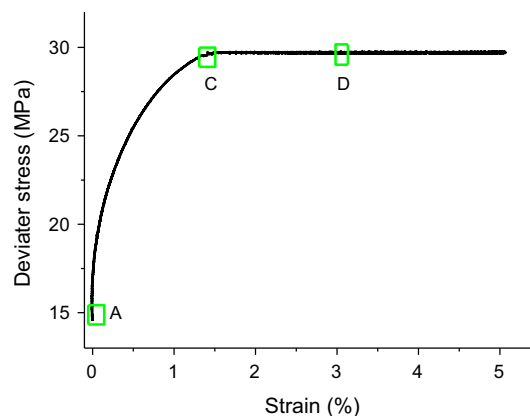
Fig. 13 Typical deviatoric stress–strain relationship under unloading test. *Note* It shows the test *curve* for the unloading and creep processes. *Point* A denotes the start of unloading, and *point* C is where unloading ends (i.e., confining pressure becomes zero). *Point* D is the transition point from initial creep to steady-state creep
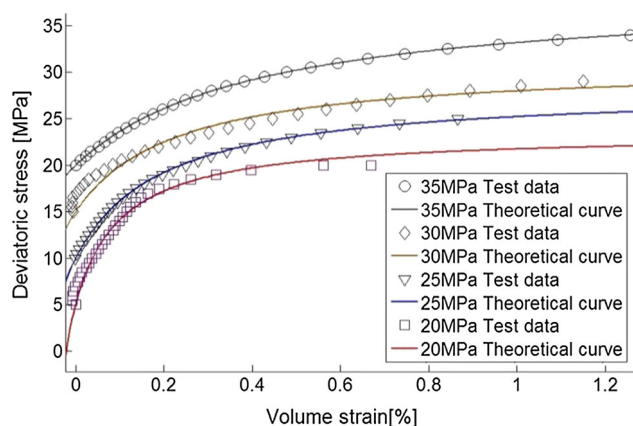
Fig. 14 Theoretical model versus testing results for rock salt

3.4.2 Creep stage

After unloading, the confining compression stress did not decrease and the axial compression stress remained unchanged; therefore, the rock salt underwent creep deformation. Because the creep mechanisms in the unloading test and in the general triaxial compression stage were the same (Ma et al. [14] and Liang et al. [13]), with respect to the steady-state creep stage. We conclude that α and β in Eq. (2) are coefficients related to loading stress and take the form:

$$\alpha = d_4\sigma \tag{10}$$

$$\beta = d_5\left(\frac{\sigma}{\sigma_m}\right)^n \tag{11}$$

where d_4, d_5, and n are constants, and σ_m is the mean stress. By substituting Eqs. (10) and (11) into Eq. (2), the creep constitutive equation in the unloading stage can be written as:

$$\varepsilon_{II} = \varepsilon_c + d_4\sigma\left(1 - \mathrm{e}^{d_3t}\right) \tag{12}$$

$$\varepsilon_{III} = \varepsilon_D + d_5\left(\frac{\sigma}{\sigma_m}\right)^n t \tag{13}$$

Equation (12) is the constitutive equation of the initial creep stage, and Eq. (13) is the constitutive equation of the steady-state creep stage.

The solid curves depicted in Fig. 14 represent the test data of the deviatoric stress–volumetric strain relationship with constant σ_3 and increasing and the dots are the theoretical results from Eq. (9). The agreement between the theoretical and experimental results is good. Equation (9) does not contain any fitting parameters, and all the involved parameters have a physical meaning.

4 Conclusions

The mechanical behaviors of dilatancy-weakened rock salt under unloading are different from those of dilatancy-weakened rock salt under uniaxial or triaxial loading because of the load-path dependency.

Rock material contains a number of randomly oriented microcracks, which are closed under loading, but reopen under unloading. The volume deformation of rock salt under unloading is greater than under triaxial loading, but is less than under uniaxial loading (with the same deviatoric stress). The dilatancy characteristics of rock salt during unloading progression are as follows.

1. The initial confining compression and initial axial compression affect dilatancy under triaxial unloading conditions, and confining pressure inhibits rock salt deformation. Under the same axial compression, the corresponding dilatancy rate decreases as the confining compression increases, and under the same confining compression, the corresponding dilatancy rate increases as the axial compression increases.

2. We found the accelerated dilatancy points at triaxial unloading confining experiment, and the boundary stress of accelerated dilatancy point is affected by confining and axial compressions. The rock salt's capacity for releasing deformation energy is weak, leading to an increase in damage. The specimens enter the creep state after the unloading process. The associated creep rate depends on the deviatoric stress and confining compression values at the end of the unloading process.

3. A damage constitutive model has been proposed for rock salt undergoing irreversible microscopic structural changes. In the model, microcracks grow as lateral confinement is reduced with constant axial stress.

References

1. Alkan H (2009) Percolation model for dilatancy-induced permeability of the excavation damaged zone in rock salt. Int J Rock Mech Min Sci 46(4):716–724

2. Alkana H, Cinarb Y, Pusch G (2007) Rock salt dilatancy boundary from combined acoustic emission and triaxial compression tests. Int J Rock Mech Min Sci 44(1):108–119

3. Carter NL, Hansen FD (1983) Creep of rock salt. Tectonophysics 92:275–333

4. Chen ZW, Lv MY, Li LX, Wang Q, Zhang XY, Liu RP (2006) Theoretical investigations on electronic and optical properties of rock-salt gallium nitride. Thin Solid Films 515(4–5):2433–2436

5. Dolezalova M (2001) Tunnel complex unloaded by a deep excavation. Comput Geotec 28(6–7):469–493

6. Elaguine D (2006) Hertzian fracture at unloading. Mech Phys Solids 54(11):2453–2473

7. Guo Y, Yang C, Fu J (2012) Experimental research on mechanical characteristics of salt rock under triaxial unloading test. Rock Soil Mech 33(3):725–730

8. Guo Y, Yang C, Mao H (2012) Mechanical properties of Jintan mine rock salt under complex stress paths. Int J Rock Mech Min Sci 56:54–61

9. Hansen FD, Mellegard KD, Senseny PE (1984) Elasticity and strength of ten natural rock salts. In: Proceedings of the first Conference on mechanical behavior of salt (Pennsylvania State University), 71–83

10. Jiang D, Qiu H, Yi L, Ren S, Chen J (2012) Similar experimental study of cavity building using large-size molded salt rock. Chin J Rock Mech Eng 31(9):1746–1755

11. Kimberley J, Ramesh KT, Barnouin O (2010) Visualization of the failure of quartz under quasistatic and dynamic compression. J Geophys Res Solid Earth 115:207–215

12. Li YP, Yang CH, Qian QH, et al (2007) Experimental research on deformation and failure characteristics of laminated salt rock. In: Proceedings of the sixth conference on the mechanical behavior of salt, (Wallner, Lux, Minkley, Hardy), 69–74

13. Liang W, Xu S, Zhao Y (2006) Experimental study on creep property of rock salt. Chin J Rock Mech Eng 25(7):1386–1390

14. Ma H (2010) Study of feasibility of rock salt underground gas storage in ultra-deep formation. Dissertation, Wuhan: Institute of Rock and Soil Mechanics Chinese Academy of Sciences

15. Malmgren L, Saiang D, Toyra J, Bodare A (2007) The excavation disturbed zone (EDZ) at Kiirunavaara mine, Sweden—by seismic measurements. J Appl Geophys 61(1):1–15

16. Spiers CJ, Carter NL (1996) Microphysics of rock salt flow in nature. In: Proceedings of the fourth conference on the mechanical behaviour of salt, (Aubertin M, Hardy Jr HR) Montreal, Clausthal, 115–28

17. Tao M, Li X, Wu C (2012) Characteristics of the unloading process of rocks under high initial stress. Comput Geotech 45(6):83–92

18. Thoms RL, Gehle RM (2000) A brief history of salt cavern. In: 8th world salt symposium, Elsevier, 1–12

19. Tonge AL, Kimberley J, Ramesh KT (2012) The mechanism of compressive unloading failure in single crystal quartz and other brittle solids. Int J Solids Struct 49(9):3923–3934

20. Weidinger P, Hampel A, Blum W, Hunsche U (1997) Creep behaviour of natural rock salt and its description with the composite model. Mater Sci Eng A 234–236(30):646–648

21. Wu G, Zhang L (2004) Studying unloading failure characteristics of a rock mass using the disturbed state concept. Int J Rock Mech Min Sci 41(3):437

22. Yang CH, Liang WG, Wei DH (2005) Investigation on possibility of energy storage in salt rock in China. Chin J Rock Mech Eng 24(24):4409–4417

23. Zhou X, Qian Q, Zhang Y (2008) The constitutive relation of crack-weakened dimensional unloading. Acta Mech Solida Sin 21(3):221–231

24. Zhou HW, Wang CP, Mishnaevsky L et al (2013) A fractional derivative approach to full creep regions in salt rock. Mech Time Depen Mater 17(3):413–425